



CO adsorption and oxidation at room temperature on graphene synthesized on atomically clean Pt(001)

Nicoleta G. Apostol, Ioana C. Bucur, George A. Lungu, Cristian A. Tache, Cristian M. Teodorescu*

National Institute of Materials Physics, Atomîștilor 405A, 077125 Măgurele, Ilfov, Romania

ARTICLE INFO

Keywords:

Nanoscale reactor
Graphene
Pt(001)
In situ characterization
XPS
CO oxidation

ABSTRACT

Carbon monoxide is adsorbed at room temperature on graphene formed on atomically clean Pt(001)–*hex* phase by chemical vapor deposition, starting with ethylene, in ultrahigh vacuum. The graphene formation is characterized *in situ* by high resolution photoelectron spectroscopy (HRPES), by low energy electron diffraction (LEED) and by near-edge X-ray absorption fine structure (NEXAFS). The formation of graphene destroys the *hex* reconstruction of Pt(001) and graphene exhibits totally in-plane sp^2 bonding. CO adsorption is characterized by HRPES and a rigid shift towards higher binding energies by about 96 meV is experienced by Pt 4f core levels, together with a shift towards lower binding energy by 36 meV of the C 1s level corresponding to graphene, while the amplitude analysis of carbon and platinum peaks suggests the intercalation of carbon oxide between graphene and the metal substrate. The presence of oxidized carbon is evidenced by a separate component in the C 1s spectrum (attributed to carbon bond to oxygen) and by the occurrence of the O 1s signal. The coverage expressed in terms of the ratio of the integral amplitudes of the carbon bond to oxygen to the amplitude of the carbon from graphene approaches 3 %, yielding a CO coverage of Pt(001) of about 0.12 monolayer. The derived atomic ratio (O 1s):(C 1s bond to O) is initially close to 1, then evolves in time towards values close to 2, which means that CO is progressively oxidized upon adsorption and irradiation with soft X-rays. The relative amount of oxygen and oxidized carbon decreases in time under irradiation with soft X-rays. Weakly bound graphene on incommensurate metal surfaces may be used as atomic scale nanoreactors for trapping and immediate oxidation of carbon monoxide.

1. Introduction

Carbon monoxide attachment and surface reactions are intensively investigated during the last century, owing to the necessity to remove it from the combustion gases or to convert it into fuels via Fischer–Tropsch synthesis or methanation [1,2]. Reactions involving carbon monoxide require the use of catalysts, and platinum is one of the most widely used since several decades owing to the Blyholder charge transfer (donation from σ electrons to the metal, back-donation of d electrons from the metal into antibonding π^* orbitals) occurring when CO is adsorbed [3]. An important point regards the fixation of this molecule on the surface of a catalyst, together with the ability to dissociate it and to ensure a sufficient surface mobility of the resulting fragments. Not surprising, early surface science studies concentrated on coverage-dependent structural changes [4], with saturation coverages ranging between 0.75–0.8 monolayers (ML) [2,4,5] to 1 ML [3]. Other effects reported in early studies pointed on the inhibition of oxygen adsorption by CO pre-adsorption [4], induction of a dipole moment for

adsorbed CO on Pt(001) (0.29 D [3] with respect to 0.11 D in gas phase [6]), weakening of the back-donation as compared to other metals from the group, stronger coupling of the 5σ orbital to the metal surface [2]. Note also that 0.75 ML seems to be some kind of ‘universal’ saturation coverage of carbon monoxide on noble metals [7].

The CO oxidation reaction on platinum proceeds at about 500 K [3,8] or even at 600–700 K [9]. After the fixation of this molecule on the surface of a catalyst via back-donation processes [2,3], one has to ensure a sufficient surface mobility of the resulting fragments [10]. It is then desirable to weaken the interaction between CO and the substrate, keeping it strong enough to ensure the molecular fixation, and ensuring an elevated CO coverage for a high reaction yield. This implies the use of surfaces with higher amount of active centers. For instance, near ambient pressure X-ray photoelectron spectroscopy (XPS) and scanning tunneling microscopy (STM) evidenced that higher CO coverage (approaching 1 ML) on a surface exhibiting reactive sites contributes to a drastic rearrangement of surface structure on stepped Pt surfaces (557) or (332), yielding nanometer-sized clusters. CO is adsorbed merely on

* Corresponding author.

E-mail address: teodorescu@infim.ro (C.M. Teodorescu).

<https://doi.org/10.1016/j.cattod.2020.02.006>

Received 11 October 2019; Received in revised form 16 January 2020; Accepted 6 February 2020

0920-5861/ © 2020 Elsevier B.V. All rights reserved.

top and bridge sites, with some amount of molecules at elevated pressures attached to low coordinated Pt atoms [11]. High amounts of CO pre-adsorbed (over 0.5 ML) were reported to decrease the rate of CO + O₂ reactions. For the same reason, the Pt(001) surface is of particular importance, due to its rich *hex* reconstruction [12] manifested in extended rows of atoms which may act as adsorption sites. In this case also, reported adsorption sites were: a-top, bridge-bound and 3-fold hollow. After CO adsorbed on Pt(001), the low energy electron diffraction (LEED) pattern exhibits a $c(2\sqrt{2} \times \sqrt{2})R45^\circ$ reconstruction, corresponding to bridge-bonded CO at 0.5 ML. For larger coverages, uniaxial compression leads to the formation of incommensurate overlayers. The CO oxidation reaction proceeds at about 500 K [8].

The advent of graphene (Gr) physics and chemistry [13], together with the ability to synthesize well-ordered graphene layers on single crystal surfaces, and in particular on platinum surfaces, opened up immediately the possibility to investigate the role of these 2D layers in surface chemistry of carbon monoxide. Very rapidly, the physico-chemistry of atomic or molecular intercalations between graphene layers and metals substrates started to develop. The principle tools to study these processes are LEED and STM for revealing structures and morphologies, XPS for determining the chemical states and the presence of adsorbates, and temperature-programmed desorption (TPD) for investigating the desorption dynamics and reaction products. High resolution XPS using synchrotron radiation promotes the investigation of the narrow C 1s peak as a good fingerprint of the corrugation state of Gr and of its interaction with the substrate. For instance, during Pt alloying on Ru(0001) surface, one observes progressive detachment of the graphene layers synthesized subsequently [14]. In addition, the C 1s peak belonging to adsorbed CO or to other oxygen-containing complexes are quite different in binding energies [15]. Another synchrotron radiation related technique is angle-dependent near-edge absorption fine structure (NEXAFS), using linearly polarized soft X-rays, employed to assess not only chemical states, but also for the in-plane orientation of σ^* and π^* bonds and, implicitly, hybridization states [16–22].

One decade ago, a Ru(0001) surface fully covered by Gr was found to be passive with respect to O₂ adsorption at room temperature and only activated at elevated temperatures (> 500 K) [23]. The adsorbed oxygen intercalates between the topmost graphene overlayer and the Ru(0001), and decouple the graphene layer from the Ru(0001) substrate, forming quasi-freestanding monolayer Gr floating on the O–Ru(0001) surface, with considerable lower modulation (0.2 Å vs. 1 Å initially) in the Moiré superstructure. Strongest O 1s signal was detected for adsorption of 360 L at 600 K, and the oxygen is removed by annealing at 800–1000 K. Selective oxidation of a Ru(0001) beneath Gr lifts the strong metal-carbon coupling and restores the characteristic Dirac cones of isolated monolayer graphene. At high temperature (820 K) under O₂ exposure (6.5 × 10⁻⁵ Pa), Gr is etched due to reactive oxygen atoms; at lower temperature (610 K) and similar pressure, one obtains selective oxidation of Ru(0001) beneath Gr, starting with the sharpest edge of Gr domains. The presence of graphene weakens the binding of chemisorbed O on Ru(0001) [24]. ‘Oxygen switching of the epitaxial graphene–metal interaction’ was studied by high resolution XPS in Ref [25]. for Gr/Ir(111). O intercalation under Gr on Ir(111) was observed at temperatures starting with 500 K and pressures 0.5 Pa. One observes also an abrupt de-intercalation by annealing at 600 K, possibly with formation of CO and CO₂, together with partial etching of graphene. Oxygen uptake on Ir(111) occurs at room temperature (without Gr) and amounts 0.38 ML. With intercalation using graphene, the saturation coverage increases up to 0.60 ML. Also, an STM study evidenced that Gr on Ru(0001) splits into fragments along line defects following water intercalation at 90 K. The decoupled graphene shows no Moiré pattern [26]. For Gr/Pt(111), CO intercalation was evidenced at pressures of 1 × 10⁻⁴ Pa, at room temperature, taking place through open channels at island edges [27]. The Moiré pattern disappears from micro-LEED. CO adsorption are observed from O 1s peaks, and the saturation CO coverage for Gr/Pt(111) was about 0.8 from that obtained

clean Pt(111). Once CO is removed, the molecules confined under Gr start to desorb even at room temperature. Density functional theory (DFT) calculations confirmed that the CO adsorption energy is weakened by the presence of Gr. Intercalation of CO at high pressure (up to 600 kPa) between Gr and Pt foils (no well-defined crystallographic orientation) was reported to weaken the Gr-substrate interaction for transfer of less defective graphene [28]. ‘CO intercalation of graphene on Ir(111) in the millibar regime’ and at room temperature was reported in Ref. [29], with the formation of the same structure as the (3√3 × 3√3)R30° reconstruction obtained after Ir(111) exposed to 1 hPa CO. After intercalation, Gr behaves as p-doped free standing graphene. CO uptake was about one half of the saturation coverage on Ir(111) in absence of Gr. The C 1s shift of Gr after intercalation was – 0.3 eV experimentally, while theoretical estimates yielded – 0.46 eV. Exposure at 1 bar and room temperature of Gr/Ru(0001) yielded, again, CO intercalation, as observed by low energy electron microscopy (LEEM), with the occurrence of one-dimensional (1D) structures [30]. One notices also the disappearance of satellite spots in LEED upon intercalation, and only blurred patterns due to ordered CO on Ru(0001) are observed in this case. The O 1s signal is stronger for Gr/Ru(0001) after CO uptake than for Ru(0001) alone. The CO coverage in this case might be close to 1 ML, and molecular desorption occurs rather abruptly at 373 K. Again in this case, the conclusion was that the adsorption energy of CO on metals is decreased in the case of intercalation under Gr.

CO adsorption/desorption and CO oxidation is observed on Pt(111) surface covered by one monolayer graphene (MLG) [30]. Gr weakens the interaction between CO and Pt and facilitates the CO oxidation with lower apparent activation energy. After CO exposure up to 600 L on 0.5 ML Gr/Pt(111), CO adsorbed on platinum on top and bridge sites was identified, together with progressive development of CO adsorbed on top sites under Gr. A confinement effect is also reported, manifested as a red shift in CO stretching frequency. CO adsorbed under Gr exhibits a sharp desorption peak at low temperature. DFT calculations yielded that the CO adsorption energy decreases from 1.74 to 1.21 eV in presence of Gr. No CO adsorption was reported for at 1 ML Gr with CO partial pressure 1.3 × 10⁻⁴ Pa, but starting only with 0.013 Pa. The Pt 4f_{7/2} surface component is unchanged upon Gr deposition. Upon CO adsorption, one notices the decrease of this surface component and occurrence of two new peaks in the Pt XPS spectrum upon CO adsorption at elevated pressures (above 1.3 hPa). Oxygen intercalation under 1 ML Gr is observed for 13 Pa O₂ pressure and above 373 K. At low temperature (525 K) the CO oxidation rate obtained was better for 1 ML Gr/Pt(111) than for Pt(111). The activation energy for CO oxidation decreases from 0.74 eV for Pt(111) to 0.56 eV for 1 ML Gr/Pt(111). The term ‘2D nanoreactor’ was proposed for the spacing between Gr and Pt(111), where CO molecule are adsorbed and oxidized.

Another result obtained recently involves water decomposition under graphene deposited on Ni(111) [31]. After dosing 10⁶ L water at room temperature, the observed components are ascribed to hydrogenated Gr plus a component decoupled from the metal by water intercalation. Hydroxyls are attached to Ni, not to C (no corresponding C 1s component is visible). C–H bending and stretching modes are visible in EELS and no C–OH vibrations are detected. By heating at 470 K, the C 1s peak evolved towards its initial shape (prior to water adsorption), also C–H vibrations disappear. TPD on pre-adsorbed D₂O evidenced the desorption of D₂ at about 442 K. Note also the possibility of creating ‘nano-blisters’ by intercalation of Ar atoms under Gr synthesized on Ni(111) [32].

More recent work was dedicated to the use of another 2D system, hexagonal boron nitride (h-BN) for the same purpose of trapping and intercalating molecules between the 2D layer and the substrate, with possibility of enhanced reaction rates [33–35]. *Ab initio* DFT theory revealed ‘feasible molecule intercalation, tunable molecule–metal interaction, and enhanced reaction activity of CO oxidation’ [36] on g-C₃N₄ exhibiting triangular pores through which O₂, CO or CO₂ might

diffuse. Hence, the concept “catalysis under 2D cover” was launched in Ref. [37].

Intercalation had also as a purpose the fabrication of a thin oxide layer to decouple Gr from its metal substrate, in view of electronic applications aiming to exploit the unique conduction properties of Gr. Intercalation of oxygen was possible even between Gr and Ni(111) with strong initial interaction, with formation of surface oxide. The Dirac cone is restored after initial strong hybridization of graphene π electrons with Ni 3d orbitals, with a slight n doping after intercalation [38]. For oxygen intercalated epitaxial graphene on Ru(0001), the oxygen coverage needed for complete Gr lifting is about 0.75 ML [39]. Another possibility to begin exploitation of the conduction properties of high quality Gr synthesized on single crystals is to synthesize silica (SiO_2) layers between Gr and the underlying single crystal metal substrate. Stepwise intercalation of Si and oxygen between Gr and Ru(0001) was reported in for the first time in Ref. [40]. In a similar way, ‘chemical gating of epitaxial graphene through ultrathin oxide layers’ was reported in Ref. [41]. These observations are a sign of silicon intercalation between Gr and Ir(111). Also, the peak positions indicate that Gr on Si is n-doped. During subsequent oxidation of this surface, the C 1s peak intensity is progressively transferred to a low BE component (shift by 0.23 eV with respect to the Gr/Ir(111) component), featuring p doping of graphene.

This work presents first results regarding CO intercalation at room temperature in the Gr/Pt(001) surface, studied by high resolution XPS. NEXAFS and LEED will also be used to characterize the surface prior to CO adsorption at room temperature. The main reasons to investigate the ability of this surface were: (i) the fact that it was shown that Gr on Pt(111) is one of the weakest Gr-metal bonds [42], and thus one expects that Gr on Pt(001) will be even weaker, owing to the incommensurate character of the Pt(001) with respect to the Gr structure; (ii) the rich *hex* reconstruction of Pt(001) [12], which could provide enhanced affinity for CO to adsorb with respect to the more compact (and without superstructure) Pt(111) surface; (iii) for practical applications in real catalytic systems, when Pt films synthesized by low-cost methods will be used in conjunction with Gr, one cannot ensure a single orientation of these films, therefore all possible crystallographic orientations of the substrate need to be investigated; (iv) in addition, CO oxidation reaction on Pt(001) occurs even at 500–800 K at 10^{-5} Torr CO pressure [9]. Previous STM studies confirmed that Gr/Pt(001) preserves the (reactive) *hex* reconstruction and protects it against reaction while O_2 dosing at pressures up to 10^{-4} hPa and CO dosing at pressures up to 10^{-6} hPa (room temperature). At higher pressures, CO is observed to intercalate under the graphene coating layer, thus lifting the reconstruction, leaving intact the Gr layer. *Ab initio* DFT calculations also proves the stability of graphene [43]. The stripe structure of the *hex* reconstruction is preserved under graphene, even across step edges and domain boundaries [44]. However, such studies need to be confirmed and supplemented by XPS analyses of the chemical states. NEXAFS will also be used to check for the complete in-plane bonding of carbon atoms forming the graphene layer and to detect if defects are present in the graphene layer.

2. Experimental

The experiments are performed in an ultrahigh vacuum installation with a base pressure in the range of 10^{-9} Pa, connected to the SuperESCA beamline at the Elettra synchrotron radiation facility in Trieste. The preparation chamber is provided with VG sputter gun and gas inlets. The analysis chamber is equipped with a VG RVL900 low energy electron diffraction (LEED) optics and a Specs Phoibos hemispherical electron energy analyzer with 150 mm radius with an in-house built delay line detector. The analyzer operated in “medium area” mode with pass energies (PE) of 4 eV for Pt 4f spectra, 2 eV for C 1s spectra, and 5 eV for O 1s spectra. The photoelectron take-off angle was $\theta = 40^\circ$. Photon energies for O 1s ($h\nu = 650$ eV) and C 1s

($h\nu = 400$ eV) were chosen such as to obtain similar kinetic energies of outgoing electrons, therefore similar electron inelastic mean free paths. For Pt 4f, the photon energy employed was $h\nu = 120$ eV, owing to the large intensity and good resolution provided by the beamline at this energy.

The Pt(001) single crystal (Goodfellow) was spot welded on a supporting insulated Mo stick close to a W filament and also a K-type thermocouple was spot welded on its rear part to ensure proper temperature measurement, then mounted on the sample manipulator with 4 degrees of freedom, with possibilities of radiative heating or by electron bombardment. After proper bakeout and outgassing, the Pt (001) crystal was sputtered with Ar^+ ions with 2 keV kinetic energy, ion current on sample 5 μA , during 15 min at two different angles (± 40 degrees off-normal, in opposite directions). Thus, the crystal was annealed during 10 h at 850 °C. After this, two new sputtering cycles of 30 min each were performed at the two angles specified, followed by a flash in temperature up to 950 °C. The crystal was then held at 300 °C, oxygen was dosed in the chamber (10^{-5} Pa) and the crystal was progressively heated at 800 °C, then cooled down, five times. The LEED pattern already exhibited good crystallinity after this treatment. Finally, the crystal was shortly treated in hydrogen (5×10^{-6} Pa, 550–600 °C) to remove the remaining surface oxygen. The final result was a sharp LEED pattern exhibiting the *hex* reconstruction of Pt(001), a Pt 4f spectrum without any additional high binding energy (BE) components and almost no carbon or oxygen contamination visible by high resolution photoelectron spectroscopy (HRPES), see next Section.

Graphene was produced *in situ* by chemical vapor deposition (CVD) by dosing ethylene at high temperature (above 700 °C) and following in real time the evolution of the C 1s spectrum. Fig. 1 presents the time evolution of ethylene pressure, sample temperature, together with the follow-up by PES of the C 1s level. The C 1s signal saturates at a given moment, which is ascribed to the completion of MLG, even by increasing the ethylene pressure up to 5×10^{-5} Pa, see Fig. 1(a). A short annealing at about 800 °C was performed after the ethylene was switched off, to encourage the ordering of MLG. The result was that C 1s exhibited a sharp peak with quite low full width at half maximum (0.23 eV) and the near-edge X-ray absorption fine structure at the C K-edge exhibited σ^* and π^* peaks totally dependent on the incidence angle, which means that practically all carbon forms in-plane sp^2 bonds [19,22]. These data are discussed in the next Section.

After the characterization of MLG/Pt(001) by LEED and HRPES, 4500 Langmuir carbon monoxide (10^{-3} Pa \times 10 min) were dosed on this surface at room temperature, then the surface was again characterized by HRPES, as described in the following.

One essential point in this work is represented by the computation of the carbon to oxygen atomic composition. While carbon atoms bond to oxygen have a distinct signature in HRPES spectra being shifted by about 2.5 eV towards higher binding energies with respect to the main peak of graphene, the computation of the [O]:[C] ratio, especially when synchrotron radiation with different excitation energies and different beam intensities are used, may become problematic. The fact that the analyzer operated with different pass energies (PE = 2 eV for C 1s and 5 eV for O 1s) complicates further the problem. As specified above, the kinetic energies of detected photoelectrons originating from C 1s and O 1s core levels is similar (about 120 ± 5 eV). A similar kinetic energy is provided by the As $2p_{1/2}$ level (BE about 1363 eV) from GaAs when excited with monochromated Al K_α radiation (1486.7 eV). Thus, the intensity calibration between different PE was carried out in a different experiment by measuring a clean GaAs(001) wafer with Al K_α radiation and we found a factor of $f = 4.0$ between the integral intensities obtained with PE = 5 eV and PE = 2 eV.

The beam intensity at different binding energies was estimated by measuring the total electron yield current produced by the electrically insulator refocusing mirror of the SX 700 type monochromator. This mirror is coated with gold [45,46], thus the total electron yield currents ($TEY(400 \text{ eV}) = 41.0$ nA at $h\nu = 400$ eV and $TEY(650 \text{ eV}) = 10.7$ nA at

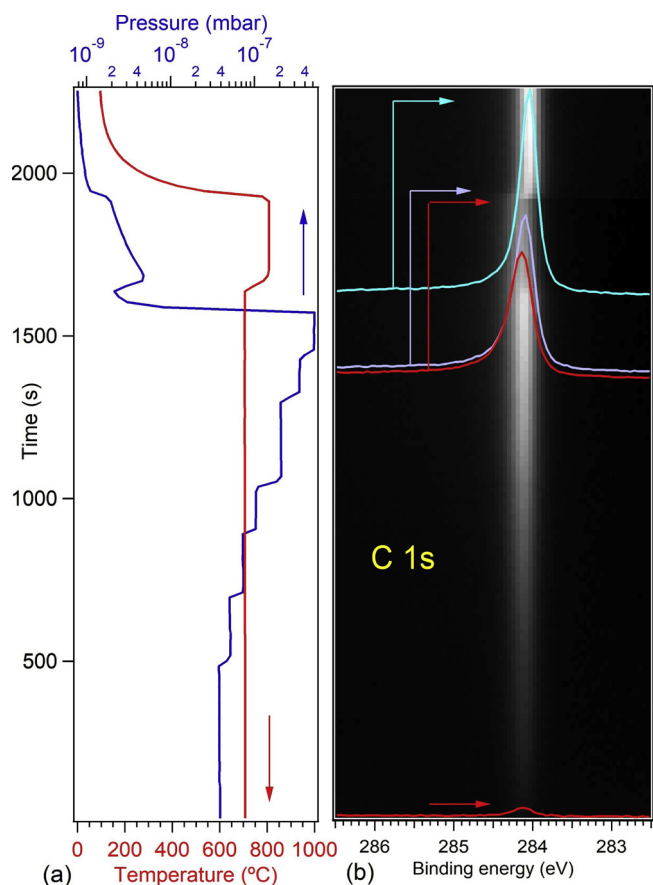


Fig. 1. *In-situ* follow-up by photoelectron spectroscopy of the graphene growth. (a) represents the time evolution of pressure (blue curve) and temperature (red curve) during the deposition. (b) represents a 2D image with the successive C 1s photoemission spectra (white represents maximum intensity). Some selected photoemission spectra are presented, recorded at different moments, denoted by arrows (For interpretation of the references to colour in this figure legend, the reader is referred to the web version of this article.).

$h\nu = 650$ eV) were re-normalized with respect to the total Au photoionization cross section computed theoretically in Ref. [47]: $\sigma_{\text{tot.}}(\text{Au}, 400 \text{ eV}) = 5.47 \text{ Mb}$ at $h\nu = 400$ eV and $\sigma_{\text{tot.}}(\text{Au}, 650 \text{ eV}) = 3.5 \text{ Mb}$ at $h\nu = 650$ eV. The integral intensities of the C 1s and O 1s spectra were also renormalized with respect to the 1s subshell photoionization cross section ($\sigma(\text{C } 1s, 400 \text{ eV}) = 0.4637 \text{ Mb}$ for C 1s at $h\nu = 400$ eV and $\sigma(\text{O } 1s, 400 \text{ eV}) = 0.3383 \text{ Mb}$ for O 1s at $h\nu = 650$ eV). Thus, ‘corrected integral amplitudes’ (CIA) used for derivation of atomic concentrations will be:

$$CIA(\text{C } 1s) = \frac{\int y_{\text{C } 1s}(E) dE}{\sigma(\text{C } 1s, 400 \text{ eV})} \times \frac{\sigma_{\text{tot.}}(\text{Au}, 400 \text{ eV})}{TEY(400 \text{ eV})} \quad (1a)$$

$$CIA(\text{O } 1s) = \frac{\int y_{\text{O } 1s}(E) dE}{f \times \sigma(\text{O } 1s, 650 \text{ eV})} \times \frac{\sigma_{\text{tot.}}(\text{Au}, 650 \text{ eV})}{TEY(650 \text{ eV})} \quad (1b)$$

where $y_{\text{C } 1s}(E)$ or $y_{\text{O } 1s}(E)$ are the C 1s or O 1s photoemission spectra and the integral is performed over regions of interest corresponding to the relevant peaks. This has to be observed with particular care for the C 1s signal, where the peak corresponding to graphene and that corresponding to C–O lie in different energy regions, i. e. 283–285 eV for C from graphene and 285.5–287.5 eV for C belonging to adsorbed carbon oxides.

The fitting of the C 1s (region corresponding to carbon bound to oxygen) and of the O 1s levels was performed by using pseudo-Voigt lineshapes and associated integral backgrounds, following analytical approximations developed in Ref. [48].

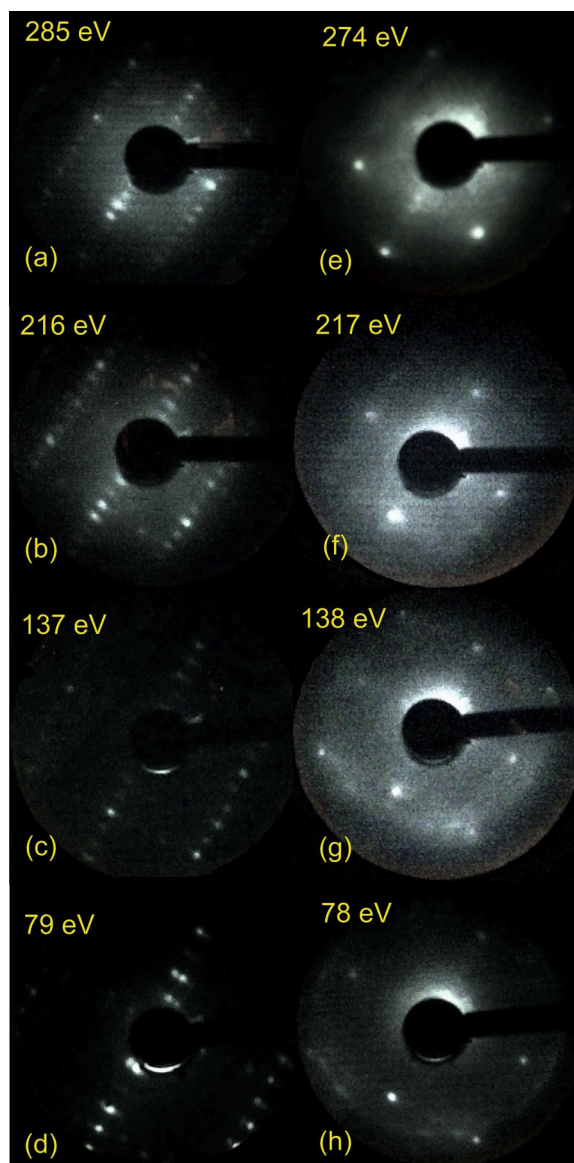


Fig. 2. Low energy electron diffraction (LEED) for Pt(001)-hex after cleaning (a–d) and after the deposition of 1 monolayer graphene (e–h). The electron kinetic energies utilized are marked on each image.

3. Results and discussion

3.1. Growth of graphene, in situ characterization and surface modification of Pt(001)

LEED patterns of Pt(001) before and after graphene deposition are represented in Fig. 2. One observes satellite peaks in LEED patterns at practically all the kinetic energies employed (Fig. 2(a–d)), which is a sign of the hex reconstruction of Pt(001) [12]. After graphene deposition, the satellite spots are no longer visible and only the 1×1 spots originating from Pt(001) are visible. However, the background increases after MLG deposition, there is also a faint circle visible in Fig. 2(g) and some weak superstructure elongated peaks are visible in the lower-left part of Fig. 2(h). These structures are due to MLG and this layer is likely to be unoriented. This result is at variance with the recently reported preservation of the hex reconstruction of Pt(001) after graphene deposition [43,44].

NEXAFS spectra recorded at various angles of incidence of the beam on the sample surface α are represented in Fig. 3. The integral

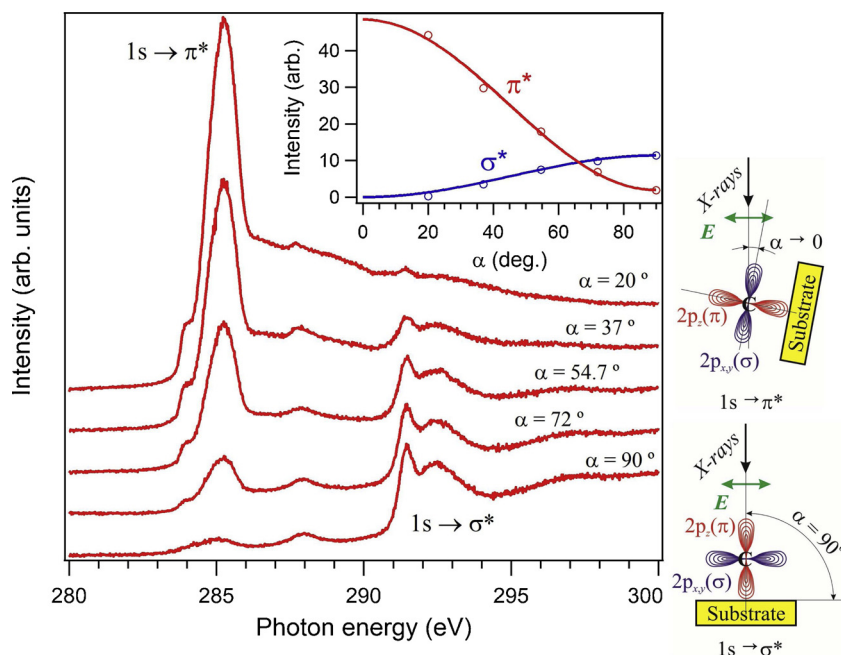


Fig. 3. Near-edge X-ray absorption fine structure (NEXAFS) at the carbon K-edge for 1 monolayer graphene grown on Pt (001). The insert represents the variation of intensities corresponding to transitions to σ^* and π^* unoccupied electronic states as function on the angle α between the direction of the soft X-rays and the sample surface. The lines are fits with $\cos^2\alpha$ for the transition to π^* and $\sin^2\alpha$ for the transition to σ^* . The drawing at the right shows the orientation of the $2p$ σ^* and π^* orbitals with respect to the linear polarization of the incoming X-rays in two extreme cases: normal incidence (bottom) and nearly grazing incidence (top).

amplitudes corresponding to transitions $1s \rightarrow \sigma^*$ and $1s \rightarrow \pi^*$ are represented in the insert. The data are well fit with $\cos^2\alpha$ and $\sin^2\alpha$ functions, which is a sign that most of the carbon $2p$ orbitals form in-plane σ bonds [16–22]. Hence, this is a sign of a ‘perfect’ local structure around carbon atoms and possibly also a sign of low corrugation. Note, however, that the ‘fingerprint region’ between σ^* and π^* resonances [19,20] exhibits some peaks, which may be due to double-vacancy or line defects. Thus, though perfect from the two-dimensional point of view, the graphene layer is prone to various defects, which may act as capture and insertion centers for carbon monoxide.

Fig. 4 presents XPS spectra. Prior to MLG synthesis, the Pt(001) crystal was atomically clean, with a contamination degree estimated below 3×10^{-4} ML. After MLG growth, the C $1s$ peak (Fig. 4(a)) exhibits a total full width at half maximum (FWHM) of 0.230 ± 0.005 eV and its position is at 284.00 ± 0.005 eV, suggests the decoupling of MLG from Pt(001). The total FWHM for C $1s$ was reported to decrease to 0.27 eV after graphene lifting by oxygen intercalation between Gr and Ni(111), which was correlated to the loss of corrugation of the Gr layer, with lower interaction with the substrate [38]. The energy position we detected is also in line with other weakly interacting graphene–metal systems. The C $1s$ BE from strongly interacting Gr with Ru (0001) is reported at 285.1 eV, while weakly interacting Gr on Pt–Ru (0001) substrate alloy is reported at 284.5 eV [14]. For Gr/Ir(111), the narrow C $1s$ peak together with its position (284.0 eV) suggests that Gr is decoupled from the substrate [25]. For CO intercalation between Gr and Ir(111), the C $1s$ BE corresponding to the Gr peak is observed at 283.8 eV [29]. Exposing to CO Gr/Ru(0001) at high pressure (starting with 13 hPa), the C $1s$ spectrum becomes dominated by a component at 283.64 eV [30]. For water decomposition under Gr/Ni(111), the C $1s$ BE for Gr/Ni(111) was 284.84 eV together with another weaker component at 284.39 eV, attributed to non-interacting carbon [31]

For oxygen intercalated epitaxial graphene on Ru(0001), the C $1s$ peaks are recorded at 284.48 eV and 285.11 eV for Gr/Ru(0001) (ascribed to distanced and close C atoms to the Ru surface, respectively) [39]. During oxygen intercalation at 450 K (0.05 Pa), the C $1s$ component starts to be dominated by a narrow peak at 283.6 eV. In conclusion, the C $1s$ BE suggest a weakly interacting Gr with Pt(001), and also its FWHM is the lowest to be ever reported, from our knowledge, implying a quite small corrugation.

The residual signal in the O $1s$ region after cleaning (insert in Fig. 4(a), blue curve) may be due to some Pt Auger signal, such as

N_1N_2V . The photon energy employed was 650 eV, therefore the electron kinetic energy is around 120 eV. The N_1 ($4s$) and the N_2 ($4p_{1/2}$) binding energies are 725.4 eV and 609.1 eV, respectively, in metal Pt [49]. There was a possibility to explore whether this small peak is residual contamination with oxygen or Pt Auger by changing the photon energy, but this was not attempted, since the data from the insert of Fig. 3(a) were performed in a time-resolved scan during the Pt(001) crystal cleaning in O_2 atmosphere. Anyway, even if there is a small contamination with oxygen, its amount would be in line with the negligible carbon contamination discussed previously. Note that most of the studies cited in the Introduction circumvent completely any residual pre-contamination of the metal single crystal surfaces.

The Pt $4f$ spectrum (Fig. 4(b)) exhibits a small shift of about 20 meV towards higher binding energies upon graphene deposition, also at variance with the result reported for Pt(111), where no shift in the Pt $4f$ level was recorded [10]. The decrease in XPS intensity of the Pt $4f_{7/2}$ peak was by 18 %, which is consistent with a $d/(\lambda\cos\theta) \approx 0.2$, where d is the attenuation depth, λ the inelastic mean free path (about 5–8 Å for electrons of around 50 eV kinetic energy) and θ the electron detection angle (40°). Hence, the derived value of d is at most 1.2 Å. After recalibration in energy and intensity, the Pt $4f_{7/2}$ signal is almost identical, which again may be a sign of a quite weak interaction between Pt and Gr. On the other hand, the loss of the *hex* reconstruction has no corresponding fingerprint in the XPS spectra. There is also a hump in the Pt $4f$ spectrum of Gr/Pt(001) before the $5/2$ line at about 73.2 eV BE and this may be interpreted as a satellite associated to the $7/2$ line, amplified by the presence of the Gr layer.

3.2. Adsorption and photodesorption of carbon monoxide

After CO dosing (4500 L), the C $1s$ spectrum is represented in Fig. 4(c) and the Pt $4f$ in Fig. 4(d). The C–O or C=O related peaks are now visible in the C $1s$ spectrum at about 286.4 eV, see the difference signal in the left insert of Fig. 4(c). Another straightforward observation is that the intensity of Pt $4f$ decreases considerably, while the intensity of C $1s$ does not decrease (on the contrary, there is a slight increase, see the insert of Fig. 3(c)). This is a clear sign of CO intercalation between Gr and Pt(001).

The ratio between integral intensities between this oxygen-related peak and the main (Gr) peak of the C $1s$ spectrum is about 2.7 %. One has to notice also that the inverse of the Gr surface atomic density

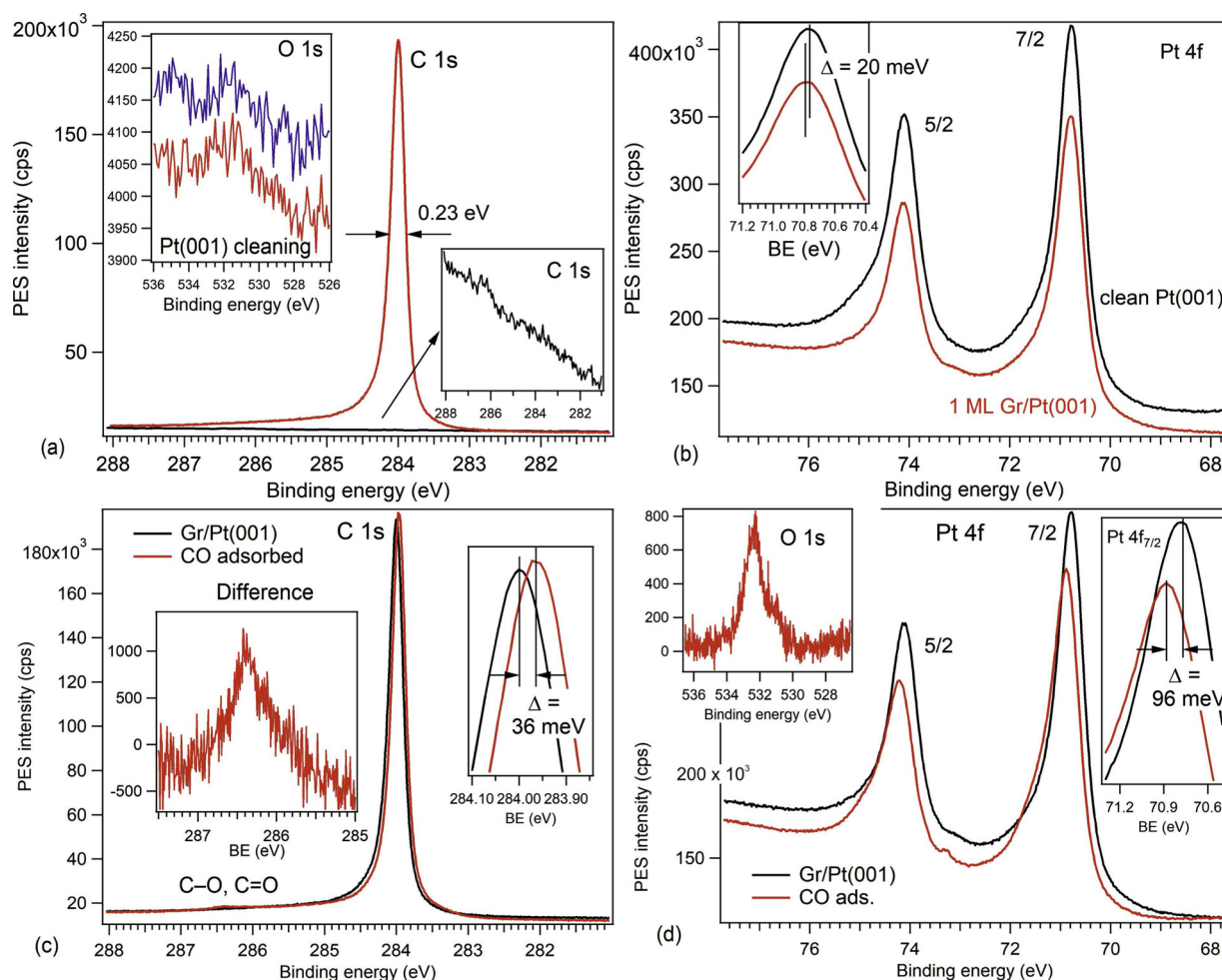


Fig. 4. Photoelectron spectroscopy analysis. (a) The C 1s spectrum for the 1 monolayer graphene grown on Pt(001), obtained with photon energy $h\nu = 400$ eV. The insert at the bottom right represents the C 1s signal from clean Pt(001). The insert at the top left represents O 1s spectra during the cleaning procedure (see text for details). (b) Pt 4f spectra for the clean Pt(001) (black curve) and for the 1 monolayer graphene deposited on it (red curve), obtained with $h\nu = 120$ eV. The insert presents a detail of the Pt $4f_{7/2}$ maximum with the estimated difference in energy between the maxima of both spectra. (c) C 1s spectra ($h\nu = 400$ eV) for 1 monolayer graphene on Pt(001) (black curve) and after the adsorption of 4500 Langmuir carbon monoxide (red curve). The insert at the left presents the difference between both spectra in the region of C 1s corresponding to C–O bonds, the insert at the right presents a detailed view of the main peaks, with the estimated difference in energy between the two maxima. (d) Pt 4f spectra ($h\nu = 120$ eV) for 1 monolayer graphene deposited on Pt(001) (black curve) compared with the spectrum obtained after adsorbing 6000 L of CO (red curve). The insert at the left represents the O 1s signal after CO adsorption, obtained with $h\nu = 650$ eV. The insert at the right presents a detail of the Pt $4f_{7/2}$ maximum with the estimated difference in energy between the maxima of both spectra (For interpretation of the references to colour in this figure legend, the reader is referred to the web version of this article).

corresponds to one atom for 2.62 \AA^2 [22], while for the unreconstructed (1×1) Pt(001) the area corresponding to one atom is about $n_s^{-1} \approx 7.68 \text{ \AA}^2$. Thus, the C(–O) coverage related to the Pt(001) surface density must be multiplied by the ration of these surface densities, i. e. by a factor of ~ 2.9 . Next, one assumes mostly “atop” adsorption sites (see below), the maximum surface adsorption sites for carbon equals at most the surface Pt atoms. Therefore, reported to this adsorption configuration, the coverage with CO becomes 8 % of a full ML. Next, one introduces the attenuation factor of this C(–O) by the Gr overlayer, similar to that derived from comparing the clean Pt(001) and for Gr/Pt(001), although the kinetic energy is different (about 113–114 eV for C 1s as compared with 49 eV for Pt 4f). From most inelastic mean free path graphs as function on the electron kinetic energy, their values for the above two kinetic energies are similar. In this case, the CO coverage amounts \sim at least $\theta_a \approx 0.08/0.82 \approx 0.1$ ML. Note that the “bridge” configurations, where an adsorption site is represented by two Pt atoms, was not considered in the above evaluation.

In fact, the ‘deconvolution’ of C 1s from the C(–O) peak and of the O 1s signal, represented in Fig. 5 reveals two peaks, a main peak with higher BE (286.4 for C 1s and 532.4 eV for O 1s) and another one with

lower BE (286.0 eV for C 1s and 531.0 eV for O 1s) whose integral amounts $\eta = 0.22$ – 0.26 from the main peak. The attribution of these peaks is CO adsorbed on “atop” configurations on platinum for the higher BE (main) peak and CO adsorbed on “bridge” sites for the lower BE (weaker) peak. A short review of the literature supports fully these attributions. For Gr/Pt(111), the CO adsorption sites are observed from O 1s peaks in XPS at 533.0 eV (atop) and 531.3 eV (bridge), with ratio $\sim 1:2$ for clean Pt(111) [27]. Also, the O 1s binding energy was 532.3 eV for Gr/Ir(111) intercalated with CO [29]. O 1s peaks are observed at 531.95 and 530.58 eV (corresponding to CO adsorbed on top and bridge sites) for Gr/Ru(0001) intercalated with CO [30]. Also, O 1s binding energies at 531.1 eV and 532.8 eV are attributed to bridge and on-top CO for CO intercalated in Gr/Pt(111) [10]. For water decomposition under Gr/Ni(111), the non-dissociated water gives the O 1s peak at 532.51 eV, while hydroxyl O 1s shows up at 530.54 eV [31]. If now one takes into account also the “bridge” adsorption sites, the total coverage is obtained as $\theta_a \times (1 + 2\eta)/1 + \eta = 0.12 \pm 0.02$ ML.

The next observation is that C 1s and Pt 4f core levels exhibit rigid shifts of 36 meV towards lower BE and by 96 meV towards higher BE, respectively. This is consistent with the prevalence of CO adsorbed on

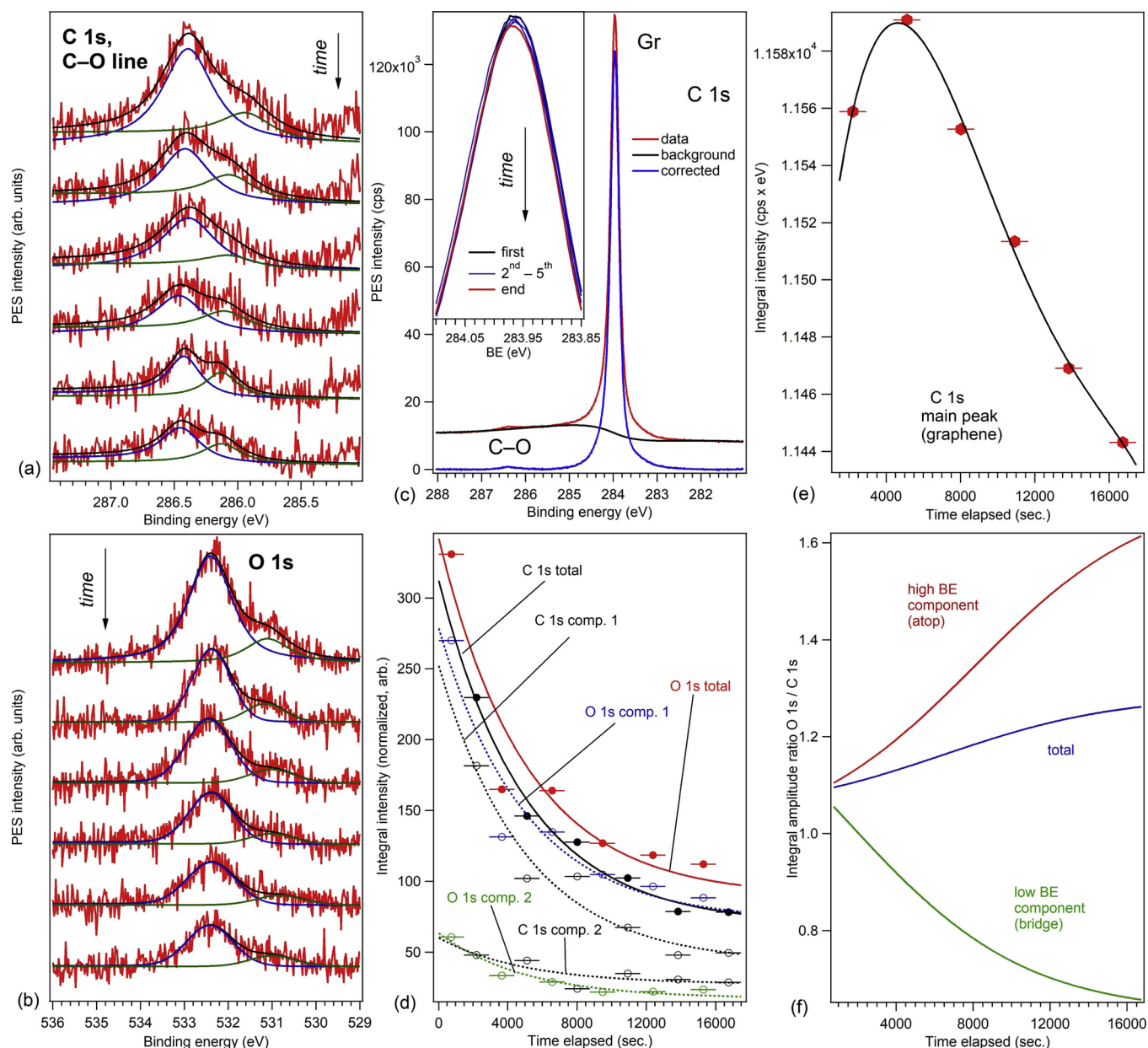


Fig. 5. (a) C 1s (photon energy $h\nu = 400$ eV, only in the region of the C–O line) and (b) O 1s ($h\nu = 650$ eV) photoelectron spectra obtained successively, after dosing 4500 Langmuir CO on graphene grown on Pt(001). The spectra are ‘deconvoluted’ each one with two Voigt lines. (c) The total C 1s signal, with a procedure for background removal, in order to evaluate its integral intensity. The insert represents the evolution of the total integral intensity of the C 1s signal corresponding to the graphene peak at about 284 eV, normalized by the photoionization cross section, the sample current and by the total Au photoionization cross section (see text for details). (d) Time evolution of integral intensities for C 1s corresponding to C–O bonding (separated components, open black circles; total integral intensity, full black circles) and for O 1s (separated components, open blue and green circles; total integral intensity, full red circles). The intensities are corrected by the photoionization cross section, the different pass energies employed and by the beam intensity, such that their ratio is similar to the atomic ratio. (e) Time evolution of the main C 1s peak. (f) Derived hypothetical time evolution of the [O]:[C] ratio, where the blue line is obtained by dividing fits of the time evolution of the total integral intensities, and the red and green lines are obtained by dividing fits of the time evolution of the components with higher and, respectively, lower binding energies from (a, b) (For interpretation of the references to colour in this figure legend, the reader is referred to the web version of this article).

top of Pt atoms, with carbon bound to platinum and being relatively positive ionized due to charge transfer processes, while oxygen becomes more negatively ionized due to back-donation. A dipole moment for a CO molecule may be estimated from this potential difference $\Delta V = 0.132$ V. Assuming that this potential difference is some kind of ‘depolarization field’ $\Delta V/d$ for the medium formed by CO trapped between Gr and Pt(001), with a polarization being given by $P \approx p \times \theta_a \times n_s/d$, where p is the CO dipole moment and d the distance between the Pt(001) surface and the graphene layer. Assuming the dielectric constant close to unit for this region, due to the relatively low density of

polarizable entities, one may then estimate the dipole moment of CO, within maximum 16 % of error (estimated with a straightforward evaluation of the dielectric constant using the Clausius-Mossotti equation and the volume polarizability of CO of 1.95 \AA^3 [6,50]):

$$p = \frac{\epsilon_0 \Delta V}{\theta_a n_s} \approx 0.27 \text{ D} \quad (2)$$

This value is in close agreement with the value of 0.29 D reported by Engel and Ertl in 1979 [3]. In conclusion, the presence of Gr has no principal influence on the charge transfer processes occurring between

CO and platinum. Note that in the above equation, the θ_a coverage employed was that corresponding only to CO adsorbed on “atop” position, about 0.1 ML.

Fig. 5 presents the time evolution of the O 1s and C 1s (structures of carbon bound to oxygen). These spectra were recorded during about 5 h, with the synchrotron radiation beam on the sample. The first observation is related to the decrease in amplitude of both peaks. The Gr peak from the C 1s also decreases in intensity (upper insert in Fig. 5(c)), but the relative decrease in intensity is of about 1.2 %. This decrease can be attributed to a slight surface heating of the sample, yielding a small displacement from the focus of the analyzer. Obviously, such mechanical or focusing effect cannot explain the decrease to about one third of the integral intensity of the C 1s and O 1s peaks represented in Fig. 5(a, b). The mechanisms yielding to the desorption of CO may be thermal and/or electronic (i. e. following the interaction with soft X-rays) and/or just a simple decay in time after dosing, with no connection to the beam irradiation. The photon flux is in the range of $2.5 \times 10^{11} \text{ s}^{-1}$, therefore at a photon energy of 400 eV through the exit slit of $10 \times 100 \mu\text{m}^2$ the power density is around $\Phi_0 \approx 16 \text{ kW m}^{-2}$. If this energy would be dissipated only radiatively, the area should be heated locally at around 730 K, according to the Stefan-Boltzmann law. If heat transfer through the sample is to be taken into account, owing to the high thermal conductivity of Pt ($\alpha = 71.6 \text{ W m}^{-1} \text{ K}^{-1}$ [6]), the temperature difference between the irradiated area and room temperature is on the order of $\Phi_0 \delta / \alpha < 0.1 \text{ K}$, where δ is a typical lateral distance of the photon flux (on the order of 10^{-4} m). As a consequence, thermal effects cannot be precluded. Moreover, in a separate experiment, an area which was not subject to previous beam irradiation was investigated after a few hours from the CO dosing and continuous measurement in X-ray beam, and the CO signal was also found to decrease with respect to its initial value immediately after dosing. These experiments are in course and will be detailed in a further work.

The time evolution of all components from the fit of the CO signal is represented in Fig. 5(d). The data were corrected from the different photon flux at the two photon energies employed, and also by the atomic photoionization cross section [47], following the procedure described in Sec. 2. All data were fitted with simple or double exponentials, with no immediate physical relevance. The composition ratio [O]:[C] obtained from the total signal is represented in Fig. 5(e). The result is that not only the total amount of adsorbed CO varies in time, but also the [O]:[C] ratio, which starts from a value close to 1 and increases in time. Moreover, if one computes separately these ratios for the “atop” and “bridge” configurations for CO adsorbed on platinum, the result, represented by red and green curves in Fig. 5(f) is that the $([O]:[C])_{\text{atop}}$ ratio increases in time to values exceeding 1.6, while the $([O]:[C])_{\text{bridge}}$ ratio decreases to values close to 0.7. One may then speculate on a reaction such as $\text{CO}_{\text{atop}} + \text{CO}_{\text{bridge}} \rightarrow \text{CO}_2 + \text{C}$, the remaining carbon integrating the Gr layer and being probably responsible for the increase in the main C 1s peak related to Gr.

4. Conclusions

This work is another proof of successful insertion of carbon monoxide between graphene and this time a new substrate, Pt(001). Despite the fact that Gr deposition yields to the loss of the *hex* reconstruction of the substrate, the interaction between Gr and Pt(001) remains weak, with no significant change in the Pt 4f_{7/2} XPS signal. CO is adsorbed most probably from defects in graphene, whose presence is suggested by the additional peak in NEXAFS between π^* and σ^* resonances. The angular dependence of σ^* and π^* resonances in NEXAFS suggest a pure two-dimensional character of the Gr layer, together with some distinct features in LEED. The amount of CO inserted is estimated to at least 0.12 ML, which is a valuable result, by taking into account the relatively low CO pressure utilized (10^{-3} Pa) and that the dosing was performed at room temperature. The shifts in BE of C 1s from graphene and Pt 4f suggest the accommodation of CO adsorbed in “atop” sites with

dipole moments of 0.27 D, similar to the value reported four decades ago for Pt(001). Hence, the presence of graphene does not influence much the attachment processes of CO on Pt(001). The novelty of this study is the time evolution of CO-related C 1s and O 1s peaks, suggesting a progressive desorption of CO, together with alterations of the [O]:[C] ratios corresponding to both adsorption sites, namely increase of this ratio for “atop” adsorbed molecules and decrease of it for molecules adsorbed on “bridge” sites. While for the definition of “atop” oxygen-rich CO one may imagine a mixture of CO and CO₂, each of them having the carbon bound to a platinum atom, the definition of a “bridge” oxygen-poor CO would imply some adsorbed carbon without any binding oxygen. One may imagine that such carbon atoms, after just having lost their oxygen, are still located in the same adsorption sites on Pt(001) and should probably induce components in the XPS spectra close to their initial position in “bridge” configurations, before the dissociation of the molecule. In addition to the reported successful insertion of CO under Gr on Pt(111) [10,27], this work suggests that Gr/platinum foils or films with no specific crystallographic orientation is prone to act as a good molecular trap of carbon monoxide for further oxidation or reduction reactions. The observed desorption of CO in time is a combined thermal and photonic effect; the relative intensity of these effects need to be further investigated.

Credit author statement

Nicoleta G. Apostol: Synchrotron radiation experiment, data analysis.

Ioana C. Bucur: Synchrotron radiation experiment, data analysis.

George A. Lungu: Synchrotron radiation experiment.

Cristian A. Tache: Synchrotron radiation experiment.

Cristian M. Teodorescu: Synchrotron radiation experiment, data analysis, interpretation, manuscript elaboration.

Declaration of Competing Interest

None.

Acknowledgements

Access to the Elettra synchrotron radiation facility was ensured through the Long Term Proposal 20130333. We acknowledge the valuable help of the SuperESCA beamline scientists Silvano Lizzit and Paolo Lacovig. This work is funded by the Romanian Ministry of Research and Innovation (RMRI) through the PN-III-P4-ID-PCCF-2016-003 and the 75PCCDI/2018 Projects and through the Operational Program Competitiveness 2014–2020 Program, Project: NANOBIO SURF-SMIS 103528. N. G. A. is funded by the Project PN-III-P1-1.1-PD-2016-1322 and acknowledges also a grant attributed by L’Oréal – UNESCO “For Women in Science”.

References

- [1] K.W. Kolasinski, *Surface Science: Foundations of Catalysis and Nanoscience*, third edition, Wiley, Chichester, 2012.
- [2] B.E. Nieuwenhuys, Correlation between work function change and degree of electron back-donation in the adsorption of carbon monoxide and nitrogen on group VIII metals, *Surf. Sci.* 105 (1981) 505–516.
- [3] T. Engel, G. Ertl, Elementary steps in the catalytic oxidation of carbon monoxide on platinum metals, *Adv. Catal.* 28 (1979) 1–78.
- [4] G. Kneringer, F.P. Netzer, Adsorption studies of oxygen and carbon monoxide on a Pt(100) surface, *Surf. Sci.* 49 (1975) 125–142.
- [5] S.-C. Chang, L.-W.H. Leung, M.J. Weaver, Comparisons between coverage-dependent infrared frequencies for carbon monoxide adsorbed on ordered Pt(111), Pt(100), and Pt(110) in electrochemical and ultrahigh-vacuum environments, *J. Phys. Chem.* 93 (1989) 5341–5345.
- [6] D.R. Lide, et al. (Ed.), *CRC Handbook of Chemistry and Physics*, 75th edition, CRC Press, Boca Raton, 1994p. 9–45, 10–196 and 12–160.
- [7] V.I. Bukhtiyarov, V.V. Kaichev, I.P. Prosvirin, X-ray photoelectron spectroscopy as a tool for in-situ study of the mechanisms of heterogeneous catalytic reactions, *Top. Catal.* 32 (2005) 3–15.

- [8] A.K. Santra, D.W. Goodman, Catalytic oxidation of CO by platinum group metals: from ultrahigh vacuum to elevated pressures, *Electrochim. Acta* 47 (2002) 3595–3609.
- [9] F. Gao, Y. Wang, Y. Cai, D.W. Goodman, CO oxidation on Pt-group metals from ultrahigh vacuum to near atmospheric pressures. 2. palladium and platinum, *J. Phys. Chem. C* 113 (2009) 174–181.
- [10] Y.X. Yao, Q. Fu, Y.Y. Zhang, X.F. Weng, H. Li, M.S. Chen, L. Jin, A.Y. Dong, R.T. Mu, P. Jiang, L. Liu, H. Bluhm, Z. Liu, S.B. Zhang, X.H. Bao, Graphene cover-promoted metal-catalyzed reactions, *Proc. Natl. Acad. Sci. U. S. A.* 111 (2014) 17023–17028.
- [11] F. Tao, S. Dag, L.-W. Wang, Z. Liu, D.R. Butcher, H. Bluhm, M. Salmeron, G.A. Somorjai, Break-up of stepped platinum catalyst surfaces by high CO coverage, *Science* 327 (2010) 850–853.
- [12] R. Hammer, K. Meinel, O. Krahn, W. Widra, Surface reconstruction of Pt(001) quantitatively revisited, *Phys. Rev. B* 94 (2016) 195406(1–11).
- [13] M. Batzill, The surface science of graphene: metal interfaces, CVD synthesis, nanoribbons, chemical modifications, and defects, *Surf. Sci. Rep.* 67 (2012) 83–115.
- [14] D. Alfè, M. Pozzo, E. Miniussi, S. Günther, P. Lacovig, S. Lizzit, R. Larciprete, B. Santos Burgos, T.O. Menteş, A. Locatelli, A. Baraldi, Fine tuning of graphene-metal adhesion by surface alloying, *Sci. Rep.* 3 (1–6) (2013) 2430.
- [15] M. Iliut, C. Leordean, V. Canpean, C.M. Teodorescu, S. Astilean, A new green, ascorbic acid-assisted method for versatile synthesis of Au-graphene hybrids as efficient surface-enhanced Raman scattering platforms, *J. Mater. Chem. C* 1 (2013) 4094–4104.
- [16] P.E. Batson, Carbon 1s near-edge-absorption fine structure in graphite, *Phys. Rev. B* 48 (1993) 2608–2610.
- [17] O. Wessely, M.I. Katsnelson, O. Eriksson, *Ab initio* theory of dynamical core-hole screening in graphite from X-ray absorption spectra, *Phys. Rev. Lett.* 94 (1–4) (2005) 167401.
- [18] A.B. Preobrajenski, M.L. Ng, A.S. Vinogradov, N. Mårtensson, Controlling graphene corrugation on lattice-mismatched substrates, *Phys. Rev. B* 78 (1–4) (2008) 073401.
- [19] E. Voloshina, R. Ovcharenko, A. Shulakov, Y. Dedkov, Theoretical description of X-ray absorption spectroscopy of the graphene-metal interfaces, *J. Chem. Phys.* 138 (1–8) (2013) 154706.
- [20] C. Ehlert, W.E.S. Unger, P. Saalfrank, C K-edge NEXAFS spectra of graphene with physical and chemical defects: a study based on density functional theory, *Phys. Chem. Chem. Phys.* 16 (2014) 14083–14095.
- [21] Y. Dedkov, E. Voloshina, Graphene growth and properties on metal substrates, *J. Phys. Condens. Matter* 27 (2015) 303002(1–28).
- [22] N.G. Apostol, G.A. Lungu, I.C. Bucur, C.A. Tache, L. Hrib, L. Pintilie, D. Macovei, C.M. Teodorescu, Non-interacting, sp^2 hybridized carbon layers on ferroelectric lead zirconate-titanate, *RSC Adv.* 6 (2016) 67883–67887.
- [23] H. Zhang, Q. Fu, Y. Cui, D.L. Tan, X.H. Bao, Growth mechanism of graphene on Ru(0001) and O_2 adsorption on the graphene/Ru(0001) surface, *J. Phys. Chem. C* 113 (2009) 8296–8301.
- [24] P. Sutter, J.T. Sadowski, E.A. Sutter, Chemistry under cover: tuning metal-graphene interaction by reactive intercalation, *J. Am. Chem. Soc.* 132 (2010) 8175–8179.
- [25] R. Larciprete, S. Ulstrup, P. Lacovig, M. Dalmiglio, M. Bianchi, F. Mazzola, L. Hornekaer, F. Orlando, A. Baraldi, P. Hofmann, S. Lizzit, Oxygen switching of the epitaxial graphene–metal interaction, *ACS Nano* 6 (2012) 9551–9558.
- [26] X.F. Feng, S. Maier, M. Salmeron, Water splits epitaxial graphene and intercalates, *J. Am. Chem. Soc.* 134 (2012) 5662–5668.
- [27] R.T. Mu, Q. Fu, L. Jin, L. Yu, G.Z. Fang, D.L. Tan, X.H. Bao, *Angew. Chem. Int. Ed.* 51 (2012) 4856–4859.
- [28] D.L. Ma, Y.F. Zhang, M.X. Liu, Q.Q. Ji, T. Gao, Y. Zhang, Z.F. Liu, Clean transfer of graphene on Pt foils mediated by a carbon monoxide intercalation process, *Nano Res.* 6 (2013) 671–678.
- [29] E. Grånäs, M. Andersen, M.A. Arman, T. Gerber, B. Hammer, J. Schnadt, J.N. Andersen, T. Michely, J. Knudsen, CO intercalation of graphene on Ir(111) in the millibar regime, *J. Phys. Chem. C* 117 (2013) 16438–16447.
- [30] L. Jin, Q. Fu, A. Dong, Y.X. Ning, Z.J. Wang, H. Bluhm, X.H. Bao, Surface chemistry of CO on Ru(0001) under the confinement of graphene cover, *J. Phys. Chem. C* 118 (2014) 12391–12398.
- [31] A. Politano, M. Cattelan, D.W. Boukhvalov, D. Campi, A. Cupolillo, S. Agnoli, N.G. Apostol, P. Lacovig, S. Lizzit, D. Farías, G. Chiarello, G. Granozzi, R. Larciprete, Unveiling the mechanisms leading to H_2 production promoted by water decomposition on epitaxial graphene at room temperature, *ACS Nano* 10 (2016) 4543–4549.
- [32] R. Larciprete, S. Colonna, F. Ronci, R. Flammini, P. Lacovig, N. Apostol, A. Politano, P. Feulner, D. Menzel, S. Lizzit, Self-assembly of graphene nanoblisters sealed to a bare metal surface, *Nano Lett.* 16 (2016) 1808–1817.
- [33] M.L. Ng, A. Shavorskiy, C. Rameshan, A. Mikkelsen, E. Lundgren, A. Preobrajenski, H. Bluhm, Reversible modification of the structural and electronic properties of a boron nitride monolayer by CO intercalation, *ChemPhysChem* 16 (2015) 923–927.
- [34] Y.H. Zhang, X.F. Weng, H. Li, H.B. Li, M.M. Wei, J.P. Xiao, Z. Liu, M.S. Chen, Q. Fu, X.H. Bao, Hexagonal boron nitride cover on Pt(111): a new route to tune molecule–metal interaction and metal-catalyzed reactions, *Nano Lett.* 15 (2015) 3616–3623.
- [35] A. Dong, Q. Fu, H. Wu, M.M. Wei, X.H. Bao, Factors controlling CO intercalation of h-BN overlayers on Ru(0001), *Phys. Chem. Chem. Phys.* 18 (2016) 24278–24284.
- [36] S.J. Wang, Y.X. Feng, M.A. Yu, Q. Wan, S. Lin, Confined catalysis in the $g\text{-C}_3\text{N}_4/\text{Pt}$ (111) interface: feasible molecule intercalation, tunable molecule–metal interaction, and enhanced reaction activity of CO oxidation, *ACS Appl. Mater. Interf.* 9 (2017) 33267–33273.
- [37] M.M. Sun, Q. Fu, L.J. Gao, Y.P. Zheng, Y.Y. Li, M.S. Chen, X.H. Bao, Catalysis under shell: improved CO oxidation reaction confined in Pt@h-BN core-shell nanoreactors, *Nano Res.* 10 (2017) 1403–1412.
- [38] L. Bignardi, P. Lacovig, M.M. Dalmiglio, F. Orlando, A. Ghafari, L. Petaccia, A. Baraldi, R. Larciprete, S. Lizzit, Key role of rotated domains in oxygen intercalation at graphene on Ni(111), *2D Mater.* 4 (2017) 025106(1–?).
- [39] S. Ulstrup, P. Lacovig, F. Orlando, D. Lizzit, L. Bignardi, M. Dalmiglio, M. Bianchi, F. Mazzola, A. Baraldi, R. Larciprete, P. Hofmann, S. Lizzit, Photoemission investigation of oxygen intercalated epitaxial graphene on Ru(0001), *Surf. Sci.* 678 (2018) 57–64.
- [40] S. Lizzit, R. Larciprete, P. Lacovig, M. Dalmiglio, F. Orlando, A. Baraldi, L. Gaemmelgaard, L. Barreto, M. Bianchi, E. Perkins, P. Hofmann, Transfer-free electrical insulation of epitaxial graphene from its metal substrate, *Nano Lett.* 12 (2012) 4503–4507.
- [41] R. Larciprete, P. Lacovig, F. Orlando, M. Dalmiglio, L. Omiciuolo, A. Baraldi, S. Lizzit, Chemical gating of epitaxial graphene through ultrathin oxide layers, *Phys. Chem. Chem. Phys.* 7 (2015) 12650–12658.
- [42] M. Gao, Y. Pan, L. Huang, H. Hu, L.Z. Zhang, H.M. Guo, S.X. Du, H.-J. Gao, Epitaxial growth and structural property of graphene on Pt(111), *Appl. Phys. Lett.* 98 (1–3) (2011) 033101.
- [43] L. Nilsson, M. Andersen, R. Balog, E. Lægsgaard, P. Hofmann, F. Besenbacher, B. Hammer, I. Stensgaard, L. Hornekaer, Graphene coatings: probing the limits of the one atom thick protection layer, *ACS Nano* 6 (2012) 10258–10266.
- [44] L. Nilsson, M. Andersen, J. Bjerre, R. Balog, B. Hammer, L. Hornekaer, I. Stensgaard, Preservation of the Pt(100) surface reconstruction after growth of a continuous layer of graphene, *Surf. Sci.* 606 (2012) 464–469.
- [45] M. Domke, T. Mandel, A. Puschmann, C. Xue, D.A. Shirley, G. Kaindl, H. Petersen, P. Kuske, Performance of the high resolution SX700/II monochromator, *Rev. Sci. Instrum.* 63 (1992) 80–89.
- [46] F. Schäfers, P. Bischoff, F. Eggenstein, A. Erko, A. Gaupp, S. Künstner, M. Mast, J.-S. Schmidt, F. Senf, F. Siewert, A. Sokolov, T. Zeschke, The at-wavelength metrology facility for UV- and XUV-reflection and diffraction optics at BESSY-II, *J. Synchr. Radiat.* 23 (2016) 67–77.
- [47] J.J. Yeh, I. Lindau, *Atomic Data Nucl. Data Tables* 32, See also (1985), pp. 1–155 <https://vuo.elettra.eu/services/elements/WebElements.html>.
- [48] C.M. Teodorescu, J.M. Esteve, R.C. Karnatak, A. El Afif, *Nucl. Instrum. Methods Phys. Res. A* 345 (1994) 141–147.
- [49] A. Thompson, et al., X-ray Data Booklet, Lawrence Berkeley National Laboratory, University of California, Berkeley, 2009.
- [50] C.M. Teodorescu, *Phys. Chem. Chem. Phys.* 17 (2015) 21302–21314.